Enhanced Conductivity of Fuel Cell Plates through Controlled Fiber Orientation

Richard H. J. Blunk and Daniel J. Lisi
Global Alternative Propulsion Center, General Motors Corp., Warren, MI 48090

Yeong-Eun Yoo and Charles L. Tucker III
Dept. of Mechanical and Industrial Engineering, University of Illinois, Urbana, IL 61801

Manufacturers of polymeric composite bipolar plates have been relying on high loadings (60 to 90 v/o) of discrete and conductive graphite/carbon filler particles to meet fuel-cell plate conductivity targets. Unfortunately, at these loadings, the plate materials are inherently brittle and result in high scrap rates and the inability to mold thin plates (less than 1 mm) required for high stack volumetric power densities. Low loadings of high-aspect-ratio conductive fillers, a fiber/flake alignment process, and a conductive-tie layer (CTL) were used to simultaneously increase the plate conductivity and toughness. The alignment process reduces the bulk resistance in the current-flow direction, and the CTL reduces the contact resistance at the plate-to-diffusion medium interface. Although a significant reduction in plate resistance is realized, high filler loadings are still required to meet conductivity targets.

Introduction

In an electrochemical reaction, the direct conversion of chemical energy into electrical energy is not limited by Carnot-cycle constraints; thus, at standard operating temperatures, the thermodynamic efficiency limit of a fuel cell engine is approximately twice that of an internal combustion (heat) engine. However, in practice, voltage losses or overpotentials exist during the operation of PEM fuel cells and reduce this efficiency advantage. Three major types of losses are observed in low-temperature PEM fuel cells: (1) activation losses—slow reaction kinetics in the cathode catalyst layer; (2) mass-transport (gas and protons) losses—failure to transport sufficient reactant to the electrodes; and (3) ohmic losses—low protonic and electronic conduction through the thickness of the polymer electrolyte and the bipolar plate, respectively (Larminie and Dicks, 2000).

A stack volumetric power density greater than 2 kW/L is required for PEM fuel cells to be viable in vehicle applications. Although large cathodic activation overpotentials (300 to 400 mV at 1 A/cm^2) currently exist and are contributing most to the total losses, not much improvement has been made over the past forty years to reduce these losses. High-temperature membrane studies have only recently been initiated in an attempt to reduce these losses. Likewise, an increased focus on new polymer electrolyte materials has only recently begun in an attempt to increase the membrane protonic conductivity at reduced relative humidity. Instead, to achieve 2 kW/L in the near future, many fuel cell manufacturers and plate suppliers have focused on reducing the losses attributed to the bipolar plate, namely reducing the mass-transport losses via an optimization in the flow field geometry and reducing the ohmic losses via a reduction in the plate thickness and resistivity.

At present membrane electrode assembly (MEA) performance levels and stack operating conditions, a plate area specific resistance of less than approximately 30 mohm·cm^2 *and* a plate thickness of less than 2 mm are required to achieve the power density target. Suppliers are attempting to meet these resistance and thickness requirements using both metal and polymer plates.

Metal plates such as titanium and stainless steel exhibit good mechanical and low gas permeation characteristics, enabling thin plates to be manufactured at high dimensional

Correspondence concerning this article should be addressed to R. H. J. Blunk.

tolerances and at low scrap rates. These metals also exhibit excellent corrosion resistance in a PEM fuel cell environment (Davies et al., 2000) because a stable and protective metal oxide film (that is, a passive film) forms on their surfaces. To make these plates conductive, the electrically insulating oxide film must be removed or its thickness reduced, and a conductive coating must then be applied to prevent growth of the oxide film. Coating imperfections such as pinholes, which expose the metal surface to the fuel cell environment, are not problematic because these pinhole areas are electrochemically stable (that is, they passivate) and represent only a small fraction of the total area for electron transport. Fuel cell manufacturers have developed such protective and conductive inorganic (Hornung and Kappelt, 1998) and organic (Fronk et al., 1999) coatings. Metal plates protected with these coatings have accumulated over approximately 1,000 h of fuel cell stack testing without any evidence of an increase in plate resistance, nor a metal ion contamination of the MEA (anode-side), although long-term durability (that is, oxide growth protection and anode plate dissolution) is still of concern and continues to be studied for both stationary (40,000 h target) and mobile (6,000 h target) applications.

In contrast, polymer plates, for the most part, exhibit good electrochemical stability in the aggressive PEM fuel cell environment (Busick and Mahlon, 1999; Balko and Lawrance, 1982) and long-term durability is not a major concern. It is, however, much more difficult to meet the resistance *and* thickness targets, and, simultaneously, obtain good mechanical properties when using polymer plates. The intrinsically insulating polymer resin must be filled with high loadings (greater than 60 v/o) of corrosion-resistant conductive particles such as carbon black and/or graphite in order to meet the resistance target. These loadings greatly exceed percolation threshold concentrations (5 to 20%) and critical pigment volume concentrations (30 to 50%) used to formulate "electrically-conductive" plastics and coatings (Sichel, 1982; Patton, 1979). It is at these critical concentrations that the electrical resistance decreases by many orders of magnitude and the material goes through an insulator-conductor transition. Unfortunately, at or above these concentrations, the material becomes brittle (Yi et al., 1998).

Many studies have been conducted with the intent of reducing the percolation threshold so that high material toughness and high conductivity can be achieved. Factors such as binder type, filler particle size/distribution (Malliaris and Turner, 1971), degree of mix (Sichel, 1982), polymer blends (Tchoudakow et al., 1996), polymer crystallinity (Zhang et al., 1996), and particulate polymer microstructure (Grunlan et al., 2001), and their effect on percolation threshold, were investigated. Although these studies were successful in reducing the percolation thresholds and in developing materials with resistivities sufficient for antistatic (10^{12} ohm·cm), electrostatic painting (10^{6} ohm·cm), and electromagnetic interference shielding (10^{1} ohm·cm) applications, these materials are not conductive enough for plate applications (10^{-2} ohm·cm). Consequently, separator plates (2.5 to 3 mm thickness) are presently formulated well beyond these critical filler concentrations and, as a result, are inherently brittle. Not much can be done to toughen the materials at such low polymer concentrations. Excessive scrap rates are observed during plate demolding, adhesive bonding, and stack assembly operations, and higher scrap rates are anticipated using these materials in thinner, targeted plate geometries.

This study investigates the use of low loadings of high-aspect-ratio conductive particles (such as carbon/graphite fibers, flakes, carbon-black aggregates, and so on), an alignment process (Blunk et al., 2001a), and a conductive-tie layer (Blunk et al., 2001b) to meet plate conductivity, thickness, and toughness targets. Fibers/flakes with finite aspect ratios are known to be 1 to 3 orders of magnitude more conductive along their long axes (Dresselhaus et al., 1988) and known to align preferentially in the direction of flow in most injection and compression molding operations due to flow-induced forces. By aligning the long and more conductive axis of discrete filler particles in the current-flow or through-thickness plate direction, smaller and fewer insulating gaps will separate the particles from one another (Carmona et al., 1984), resulting in a material resistivity reduction and, in turn, a conductivity enhancement in that same direction. This enables the resistance target to be achieved at lower filler concentrations, and, thus, at higher material toughness levels. A novel conductive-tie layer approach is then used to reduce the resulting high contact resistances, which are attributed to the lower surface concentration of conductive particles.

This study consists of two parts. In the first, we tailor numerically the geometry of the bipolar plate, within certain design constraints, so as to maximize the amount of orientation in the through-plane direction. In the second, we compression mold several plate materials to this optimal plate geometry and measure their resistances (with and without a conductive-tie layer) to quantify the contact and bulk resistance contributions. We then assess whether the alignment process and the conductive-tie layer can reduce the plate resistivity and plate contact resistance to levels required to produce PEM separator plates with superior mechanical properties.

Numerical Study

Concept

The objective of this section is to find optimal plate geometries, using a computer simulation of flow and fiber orientation, in order to maximize the through-thickness electrical conductivity of PEM fuel cell separator plates. The main software tools are the FIDAP finite-element program for fluid flow (Engelman, 1993), together with an extensive set of user subroutines developed at the University of Illinois (VerWeyst, 1998; VerWeyst et al., 1999).

Extensive studies have been performed on fiber orientation in injection and compression molding (VerWeyst et al., 1999). In injection molding the fiber orientation is most affected by the shape of the mold cavity. For example, on a molded plate with a rib, the fibers near the rib base are aligned in the thickness direction, as shown in Figure 1. By selecting a plate geometry having offsetting channels or a periodic arrangement of grooves and lands, we may be able to get a significant amount of alignment between the top and bottom land regions of the plate, where high conductivity is needed. The concept is to tailor the details of this geometry, and also to add additional material above the lands, to create a desirable fiber orientation pattern when the plate is molded. Figure 2 shows this idea. The additional material will be re-

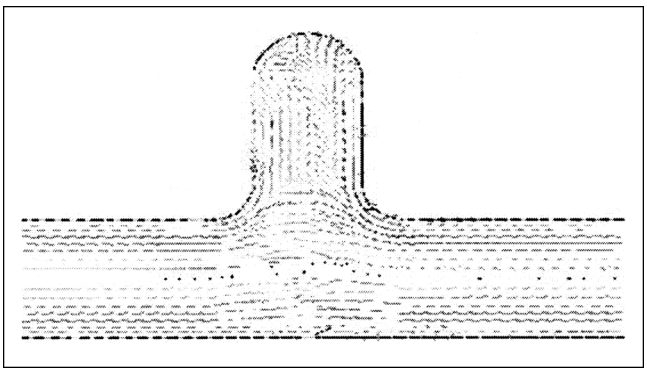

Figure 1. Example of fiber orientation near a rib.
From VerWeyst et al. (1999).

moved after molding to reveal the lands, so the amount of extra land material should be as small as possible. Two of these plates (anode and cathode) are then bonded together using a conductive adhesive to produce the interior cooling channels. Hence, the plate thickness must be less than 1 mm in order to meet the 2 mm thickness target for a cooled plate.

Note that the material removal step also decreases the plate thickness to the desired value, removes any insulating polymer-rich layer or "polymer skin" at the plate surface, thereby exposing the conductive filler, and removes the poorly aligned fibers near the surface of the extra land regions. Although this removal step is undesirable, most composite plates, including highly filled ones, also require a machining process to remove the insulating polymer skin.

Generation of trial geometries

Figure 3 shows a cross-section of the initial design for a bipolar plate. In the subsequent discussion this design will be labeled B0. This plate has a staggered pattern of grooves on the top and bottom. The up-and-down flow pattern associated with these grooves in fact provides an excellent opportunity to generate a desirable fiber orientation pattern. We want to improve fiber orientation by adjusting the size and shape of the grooves, and by adding some additional material in the land region. This latter material will be removed before the plate is used.

The grooves in a separator plate have a regular pattern that can be represented by a few parameters. We choose here

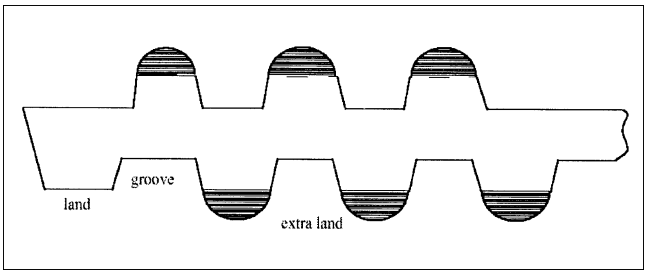

Figure 2. Separator plate with extra material in the land regions.
The shaded material is removed after molding by sanding or machining.

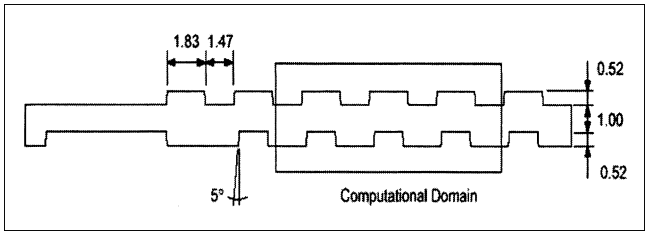

Figure 3. Initial plate geometry and its computational domain.
Linear dimensions are in millimeters.

several shape parameters to define the separator plate geometry. These parameters reflect specific geometric features of the plate, and they are quantities that we expect will have a significant effect on fiber orientation. We will examine the effects of plate shape and fiber orientation systematically, by assigning high and low values to these parameters.

Geometric parameters

We have chosen seven parameters to represent the bipolar plate geometry: (1) total thickness; (2) groove angle; (3) land length; (4) groove length; (5) groove depth; (6) groove stem depth; and (7) extra land height.

These quantities are defined in Figure 4. The amount of extra material in the land region is determined by the extra land height. The stem depth of the groove is introduced to control the roundness of the groove bottom. The groove angle provides some draft, to aid moldability. When the values for these parameters are assigned, other requirements, such as moldability, have to be considered, and the geometry generated from these parameters must also be realistic. For example, a deeper groove may be better for fiber orientation, but also may result in a thin web thickness and, in turn, excessive H_2 permeation rates and scrap rates.

Selection of trial designs

To restrict the number of designs that must be tested, the total thickness and the groove angle were fixed at 2 mm and 5°, respectively. High and low values were assigned to the other parameters, and these values are shown in Table 1. Among the five remaining parameters, a deeper groove and a higher extra land should be better for fiber orientation in the

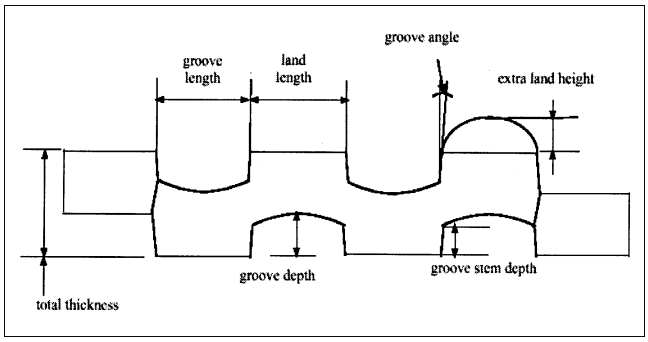

Figure 4. Parameters used to define plate geometry.

Table 1. High and Low Values for the Geometric Parameters

Parameter	Low (mm)	High (mm)
Land length	1.5	2.0
Groove length	1.5	2.0
Groove depth	0.5	0.8
Groove stem depth	0.3	0.7
Extra land height	0.0	0.7

Table 2. Parameter Selections for First Eight Trial Plate Designs

	Low Land Groove		High Land Groove	
Groove stem depth	Low	High	Low	High
Low	B2	B8	B4	B6
High	B1	B7	B3	B5

thickness direction, as long as we do not violate other requirements. For our first set of trials, we fixed these two parameters at their high values. Now, only three parameters remain, and we can examine all possible combinations. This generates eight different designs, which are labeled B1 to B8. The parameters for these designs are shown in Table 2.

To investigate the effect of the extra land height, designs with different extra land height were generated. These designs were based on the B3, B4, and B6 designs, which turned out to be the better designs among the first eight trial designs. Extra land heights ranged from 0 to 1.0 mm, at 0.1 mm increments.

Numerical analysis

FIDAP, a commercial software for general fluid problems using the Galerkin finite-element method, is used to solve the governing equations. The continuity, momentum, and energy equations are built into FIDAP, while the fiber orientation equations are incorporated through user subroutines (Advani and Tucker, 1987; VerWeyst et al., 1999).

To solve the resulting nonlinear equations, either a successive substitution or a Newton-Raphson method is used. As the problem becomes more complex, the Newton-Raphson method is preferred due to its quadratic terminal convergence and the ability to couple equations for different degrees of freedom during each iteration. The disadvantage is its small radius of convergence as compared to linear methods such as successive substitution. For coupled flow and fiber orientation, the effects of fiber orientation enter into the momentum equation through the extra stress. When the Newton-Raphson method is used, the contributions to the tangent stiffness matrix due to this extra stress and fiber orientation equation must be supplied through user subroutines.

The fiber orientation equation is a purely advective equation with no spatial diffusion, and this may make its numerical solution unstable. The streamline upwinding scheme (Brooks and Hughes, 1982) is a general method to stabilize the advective terms in this type of equation, and is used here.

Fiber orientation description

The orientation of a single rigid, axisymmetric fiber can be described by a unit vector $\boldsymbol{p}$ directed along its length. However, it is not practical to describe every fiber using this unit vector because a short fiber composite typically consists of about 10,000 fibers per cubic millimeter oriented in a multitude of directions. A concise representation of the fiber orientation at any material point is given by the second-order fiber orientation tensor $\boldsymbol{a}$, defined as

$$\boldsymbol{a} = \int (\boldsymbol{p} \otimes \boldsymbol{p}) \psi(\boldsymbol{p}) d\boldsymbol{p} \tag{1}$$

where $(\boldsymbol{p} \otimes \boldsymbol{p})$ is the tensor product of $\boldsymbol{p}$ with itself and $\psi(\boldsymbol{p})$ is the probability density function for fiber orientation. This is defined such that the probability of a fiber lying within a range $\boldsymbol{p}$ and $(\boldsymbol{p} + d\boldsymbol{p})$ equals $\psi(\boldsymbol{p})d\boldsymbol{p}$. For example, if all the fibers were aligned perfectly in the "1" direction, the a_{11} component of the orientation tensor would equal unity and all other components would be null. A completely isotropic material (that is, random fiber orientation) would have the diagonal components a_{11} and a_{22} equal to 0.5 in a two-dimensional (2-D) coordinate system. The other components would be null.

Similar to Eq. 1, the fourth-order orientation tensor is defined as

$$\boldsymbol{A} = \int (\boldsymbol{p} \otimes \boldsymbol{p} \otimes \boldsymbol{p} \otimes \boldsymbol{p}) \psi(\boldsymbol{p}) d\boldsymbol{p} \tag{2}$$

Governing equations

The filling process of injection molding is transient and includes nonisothermal and non-Newtonian effects. Fiber orientation is coupled with flow. In this work, we assume the fluid is incompressible and gravitational body forces are negligible. As a result, the appropriate forms of the continuity, momentum, and fiber orientation equations are

$$\frac{\partial u_i}{\partial x_i} = 0 \tag{3}$$

$$\rho\left(\frac{\partial u_i}{\partial t} + u_i \frac{\partial u_i}{\partial x_j}\right) = -\frac{\partial p}{\partial x_i} + \frac{\partial \tau_{ij}}{\partial x_j} \tag{4}$$

$$\frac{\partial a_{ij}}{\partial t} + u_k \frac{\partial a_{ij}}{\partial x_k} = a_{ik}\Omega_{kj} - \Omega_{ik}a_{kj} + \lambda\left(a_{ik}E_{kj} + E_{ik}a_{kj} - 2A_{ijkl}E_{kl}\right) + 2C_I\dot{\gamma}\left(\delta_{ij} - 3a_{ij}\right) \tag{5}$$

Here, u_i is the ith component of velocity, ρ is the density, and p is the pressure. In the fiber orientation equation, a_{ij} is the component of the second-order orientation tensor, Ω_{ij} and E_{ij} are the vorticity and rate-of-deformation tensors, C_I is a dimensionless constant called the interaction coefficient, and $\dot{\gamma}$ is the scalar strain rate, defined as

$$\dot{\gamma} = \sqrt{2E_{ij}E_{ji}} \tag{6}$$

The presence of the fourth-order tensor $\boldsymbol{A}$ in Eq. 5 represents a problem in obtaining a closed-form solution, since it contains unknown higher-order information. The standard approach is to approximate the fourth-order tensor in terms of the known second-order tensor using a closure approxima-

tion. In this work, the orthotropic closure approximation is adopted (Cintra and Tucker, 1995), and we use the coefficients as reported by VerWeyst (1998).

Evaluation procedure

The evaluation of each design involves two steps. First, we model the flow in the mold and predict the resulting fiber orientation pattern. Then, we relate that orientation pattern to the electrical performance of the design.

Fiber orientation evaluation

Practical injection molding involves a moving flow front, as well as nonisothermal and non-Newtonian effects. While we can perform numerical calculation considering these effects, such a task is very time-consuming, perhaps taking several days to simulate each trial design. Therefore, we simplified the problem to isothermal and Newtonian flow, and assumed that each cavity was already filled with molten polymer that flows continuously from the inlet to the outlet. This is a useful approximation, since the geometry of the flow domain is the main factor that affects fiber orientation. For this simplified problem, it still takes a few hours to complete the calculation for each design.

For these calculations, each plate design is reduced to three or two lands and grooves on each side, together with short entrance and exit regions. Trial calculations on larger geometries showed that the fiber orientation pattern is quickly established in the first set of grooves and lands, so it is not necessary to have more grooves in our analysis model. In each of these meshes the inlet is on the lefthand side, the exit is on the righthand side, and the remaining surfaces are solid walls. The plate is very long in the direction perpendicular to the page, so a 2-D analysis is performed.

The boundary and initial conditions for isothermal Newtonian flow are as follows. At the inlet, we have

$$u_x = 1 \tag{7}$$

$$u_y = 0 \tag{8}$$

$$a_{11} = 0.5 \tag{9}$$

$$a_{22} = 0.3 \tag{10}$$

$$a_{12} = 0.0 \tag{11}$$

while on all the solid walls we impose the no-slip condition

$$u_x = u_y = 0 \tag{12}$$

The exit plane is traction-free. The initial conditions, which are imposed over the entire region, are

$$u_x = 1 \tag{13}$$

$$u_y = 0 \tag{14}$$

$$a_{11} = 0.5 \tag{15}$$

$$a_{22} = 0.3 \tag{16}$$

$$a_{12} = 0.0 \tag{17}$$

Here u_x and u_y are the components of fluid velocity, and a_{11}, a_{12}, and a_{22} are the variables that describe the fiber orientation.

Current density to evaluate design

The results of the fiber orientation analysis do not immediately show which design is better. In order to evaluate the relative performance of each design, we performed a second finite-element calculation, which simulated the flow of current across the plate thickness. This calculation takes into account the orientation of the fibers at different positions on the cross-section, and the effect of this orientation on electrical conductivity. We can obtain current density q along the lands of the anode side by solving an anisotropic potential equation. For a given potential difference, the plate giving the largest current density is the best design.

The governing equation for steady-state anisotropic conduction is

$$\frac{\partial}{\partial x}\left(k_{xx}\frac{\partial u}{\partial x}+k_{xy}\frac{\partial u}{\partial y}\right)+\frac{\partial}{\partial y}\left(k_{yx}\frac{\partial u}{\partial x}+k_{yy}\frac{\partial u}{\partial y}\right)=0 \tag{18}$$

where u is the voltage (electrical potential) and k_{xx}, k_{xy}, k_{yx}, and k_{yy} are the components of the anisotropic electrical conductivity tensor. This anisotropic electrical conductivity tensor depends strongly on fiber orientation. Using the ideas of orientation averaging (Advani and Tucker, 1987), we related this conductivity tensor to fiber orientation as follows

$$\begin{pmatrix} k_{xx} & k_{xy} \\ k_{yx} & k_{yy} \end{pmatrix} = K_a \begin{pmatrix} a_{xx} & a_{xy} \\ a_{yx} & a_{yy} \end{pmatrix} + K_t \begin{pmatrix} 1-a_{xx} & -a_{xy} \\ -a_{yx} & 1-a_{yy} \end{pmatrix} \tag{19}$$

where K_a and K_t are the axial and transverse electrical conductivity of a hypothetical composite with perfectly aligned fibers. However, physical values for these coefficients are not presently available and will depend on the final material that is chosen. The main goal of this project is to compare designs to determine which design is best. For any given value of K_a, the relative performance of any design depends on the ratio K_t/K_a. We selected three values of this ratio, $K_t/K_a - 0.1$, 0.01, and 0.001, and evaluated the relative performance of each design. If a given design is best in all three cases, then it is almost certainly best for any value of K_t/K_a.

The domain for evaluation of current density was chosen as one cycle of groove and land (Figure 5). The bound conditions are

$$u = 1 \text{ on cathode} \tag{20}$$

$$u = 0 \text{ on anode} \tag{21}$$

$$u_{\text{left}} = u_{\text{right}} \text{ on periodic boundary} \tag{22}$$

$$\frac{\partial u}{\partial n} = 0 \text{ on others} \tag{23}$$

The current Q is calculated along the land region

$$Q = \int_\Gamma \boldsymbol{K}\cdot\nabla u\cdot\boldsymbol{n}ds \tag{24}$$

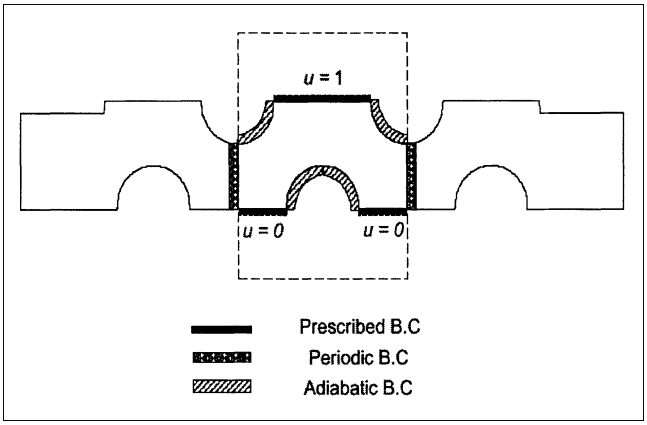

Figure 5. Calculation domain for current density.

where $\boldsymbol{n}$ is the normal vector to the boundary. Then, the current Q is divided by the length of one cycle of land and groove to obtain the current density q

$$q = \frac{Q}{\text{land} + \text{groove}} \tag{25}$$

q is proportional to the current per unit plate area for a given voltage difference, and is used to evaluate each design. The design with the largest current density is the best electrical conductor.

Results and discussion (numerical study)

In the fiber orientation results that follow, a short line is drawn at each node to represent the fiber orientation pattern. The direction of this line indicates the direction of major orientation at that point in the part, while the length of the line indicates how strongly the fibers are aligned around that direction. Thus, a long line indicates almost perfect alignment in the direction of the line and a short line indicates almost random fibers in the neighborhood. The outline in each figure shows the overall geometry that was analyzed, but the fiber orientation results are drawn only in those regions that we use to compute current density.

The simulation results for the initial B0 geometry are shown in Figure 6. We can see that most of the fibers are aligned in the plane of the plate, so the value of q is quite small. This is the expected result: the initial design is not very good.

The orientation results and the values of $q_{0.1}$ (the value of q when $K_t/K_a = 0.1$) for the B4 trial design are plotted in Figure 7. The B4 design was best, providing the largest q. An example current flux plot is shown in Figure 8. In Figure 8 the contours are lines of constant voltage and the arrows give the local current flux. Longer arrows mean greater conduction. The arrows are not perpendicular to the contours, because the conductivity is anisotropic. We see that the orientation in some specific region is quite important to the conductivity, while other regions are unimportant. This points out the importance of the current density calculation for comparing designs.

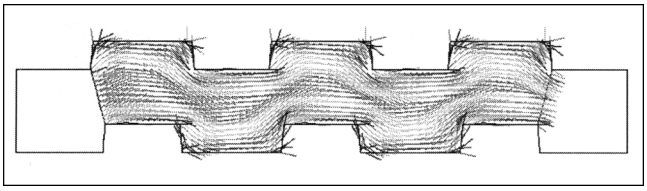

Figure 6. Fiber orientation for the initial design B0.
$q_{0.1} = 0.0734$.

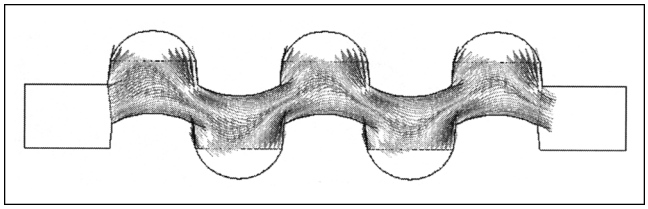

Figure 7. Fiber orientation for the optimal design B4.
$q_{0.1} = 0.1293$.

The current density values are summarized in Table 3 and Figure 9. All of the modified designs give better results than the initial design, and the current density calculations show a consistent ranking regardless of the value of K_t/K_a. Among these eight designs, the B4 design is the best. Its value of $q_{0.1}$ is 0.1293, which is about 76% greater than the value of 0.0734 for the original B0 design. As shown in Table 4, the relative increase of current density becomes much larger when we use 0.01 or 0.001 for K_t/K_a. In general, we see that smaller groove stem depth, narrower grooves, and wider lands produce better fiber orientation results.

The data shown in Figure 9 can be easily misinterpreted. They simply indicate that the designs B1 through B8 are better than design B0, regardless of the ratio K_t/K_a (for $K_a > K_t$). They are not meant to be used in determining the effect of K_t/K_a on q (that is, q does not necessarily increase with increasing K_t/K_a, as shown). These data were calculated by varying K_t for a given value of K_a. If K_t increases the overall conductivity of the composite increases, which in turn, increases q. If, instead, K_a was varied and K_t was held constant, the opposite trend would be shown—q would decrease with increasing K_t/K_a.

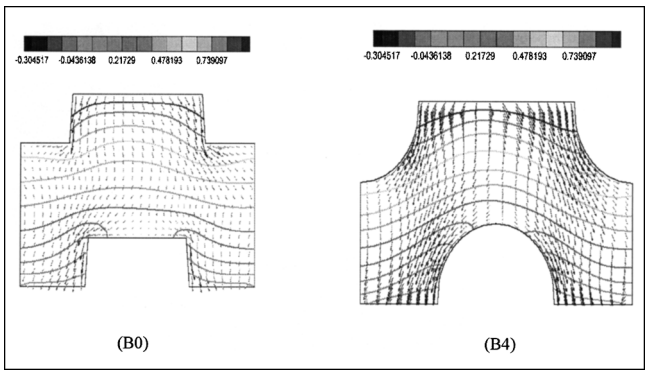

Figure 8. Examples of current flux plot for designs B0 and B4.

Table 3. Values of Current Density q for the Eight Trial Plate Designs

		Low Land Groove		High Land Groove	
Groove stem depth	K_t/K_a	Low	High	Low	High
Low	0.1	0.1128	0.0979	0.1293	0.1132
	0.01	0.0718	0.0615	0.0858	0.0738
	0.001	0.0662	0.0562	0.0799	0.0681
High	0.1	0.1039	0.0873	0.1242	0.1069
	0.01	0.0641	0.0552	0.0816	0.0724
	0.001	0.0585	0.0504	0.0757	0.0673

Based on the B3, B4 and B6 designs, we investigated the effects of the extra land height. The results are plotted in Figure 10. As we increase the extra land height, the current density increases monotonically, but the rate of increase decreases as the extra land height increases. For a 2 mm plate, 0.5 mm is about the largest extra land height that should be used.

Experimental Study

Three sets of experiments were conducted. The first uses two flat-plate designs (1 and 2 mm thickness) that are expected to generate samples having the lowest through-plane and highest in-plane conductivities because the flat samples do not contain molded grooves for enhanced through-plane alignment. The resistances of flat samples are measured and used to calculate the transverse and axial resistivities of the plate materials used in this study. These resistances are then compared with those measured from the B0 and B4 designs. The second uses the B0 and B4 designs (2 mm thickness) and determines whether a conductivity enhancement is achieved with the latter, as predicted numerically. The third uses a thinner B4 design (1 mm thickness) and determines whether the resistance and thickness targets can be achieved.

Equipment and materials

Two 10 cm $\times$ 10 cm compression mold inserts and one mold base were used (Northern Illinois Mold Corp.). The inserts

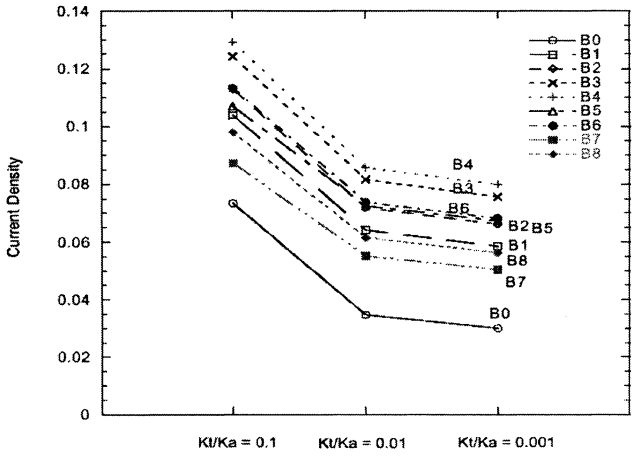

Figure 9. Evaluation for the eight trial plate designs.

Table 4. Current Density q Designs B0 vs. B4

K_t/K_a	B0	B4	Improvement
0.1	0.0734	0.1293	76 %
0.01	0.0347	0.0858	147 %
0.001	0.0300	0.0799	166 %

are made of chrome-plated hardened steel and contain ejector pins to facilitate part removal. The 2 mm insert contains both designs (half B0 and half B4) and produces a 2 mm thick part. An extra land height of 0.70 mm was used with the B4 design. The 1 mm insert contains the B4 geometry only and produces the desired 1 mm part thickness. It has a smaller 0.35 mm extra land height. Numerical trials indicated that the orientation pattern remains nearly the same if the vertical features of the plate, such as land height, groove depth, and so on, are scaled linearly with plate thickness. Planar dimensions, such as land and groove lengths, remain constant with changing plate thickness.

Six materials were used in this study, and are listed in Table 5. The first three materials contain a thermoplastic polypropylene PP binder (Montell Pro-fax 6301) and various amounts of carbon/graphite fillers, including PAN-based carbon fibers (Zoltex MF 30; 150 to 200 μm), vapor-phase-grown graphite fibers (Applied Sciences PR-11; 10 to 15 μm), and carbon black (Akzo EC300 Ketjenblack). The materials compounded with these fillers are designated PAN, PG, and CB, respectively. The remaining three materials contain a thermosetting poly vinyl ester PVE binder and various amounts of graphite flakes and/or fibers. Large (LGF: 1 mm $\times$ 1 mm) and small (SGF: 25 μm $\times$ 75 μm) graphite flakes, and long (1.2 cm) graphite fibers were selected. These materials were selected to investigate the effect of filler concentration and material anisotropy on plate resistance.

Molding procedure

In the first set of experiments, the PP-based materials were compression molded at 180°C and 17.2 MPa using the 1 mm and 2 mm flat molds. The PVE-based materials were molded similarly, but cured at 150°C for 5 min. In the second set, PP-based materials were compression molded into a 1.3 cm $\times$ 10 cm charge pattern. The charge was then positioned in

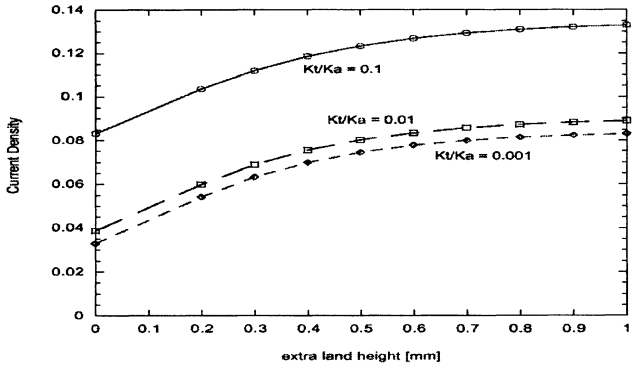

Figure 10. Current density results for various extra land heights.

Table 5. Materials Used in Experimental Study

Material Designation	Carbon Filler (vol. %)	Material Composition (vol. %)
EZ	50	15 PG/5 CB/30 PAN/50 PP
PG15	20	15 PG/5 CB/75 PP
PAN	40	40 PAN/60 PP
A	59	49 SGF/10 CF/41 PVE
B	70	70 GFL/30 PVE
C	85	85 GFS/15 PVE

PG = vapor-phase-grown graphite fiber; CB = carbon black; PAN = PAN-based carbon fiber; PP = polypropylene; LGF = large graphite flake; SGF = small graphite flake; PVE = poly vinyl ester.

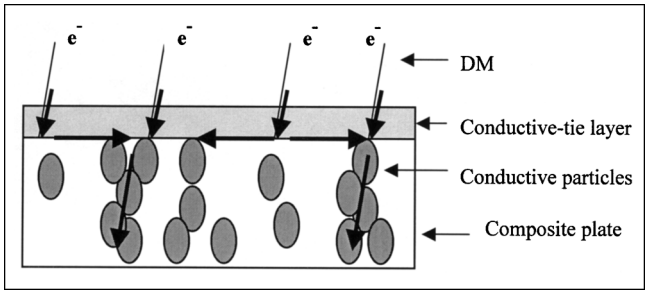

Figure 11. Conductive-tie layer (CTL) mechanism.

the center of the 2 mm insert with the long dimension of the charge parallel with that of the grooves and lands. This charge placement enables the material to flow up and down in a zig-zag fashion along the lengths of the lands and grooves, thereby increasing the through-plane alignment. In the third set, a 10 cm × 10 cm × 1.0 mm charge pattern was used. It turns out, as the results section will indicate, that not much "flow" is required to deform and align the material in the desired land-to-land direction. Here, we compression molded the PP- and PVE-based materials to a 1.0 mm thickness in order to achieve high in-plane (biaxial) and low through-plane orientation. For the PVE-based materials, this was done at room temperature to prevent cure. The charge was then placed over the entire area of the mold insert and pressed. The high in-plane orientation in the charge is, in effect, tilted upwards and downwards and becomes the land-to-land orientation in the part. This molding process is essentially a "stamping" or "forming" process, where high productivity can be achieved. The charge is either compression molded or extruded into large sheets, cut into plate dimensions, and then "stamped" in the alignment mold.

Resistance measurement process

The resistance of the plate materials should be measured at "stack conditions," namely the sample should contain flow field channels and should be sandwiched and compressed at stack pressures between two pieces of diffusion media (DM). The plate resistance is the sum of the bulk material resistance and the pressure-dependent contact resistances located at the two DM/plate interfaces. The resistance is measured using a four-point method and calculated from measured voltage drops and from known applied currents and sample dimensions. The voltage drop is measured across either the two diffusion media (total resistance) or two points on the plate surface (bulk resistance). For the former, thick DM (1.0 mm, Toray TGP-H-1.0T) is used so that needlelike voltage probes can make contact easily with the DM. The contact resistance is the total resistance less the bulk resistance.

Conductive-tie layer

The contact resistance (CR) at the DM/plate interface is significant and usually contributes more to the total plate resistance than does the bulk resistivity, particularly at low compression pressures. CR is not clearly understood because it depends on so many factors such as bulk conductivity, sample flatness and roughness, pressure, and surface composition. It is clear, however, that the CR must be reduced in order to meet the resistance target at reduced filler loadings and at low stack pressures.

The CR at the DM/plate interface can be reduced significantly with the use of a conductive-tie layer. Figure 11 illustrates the conductive-tie layer mechanism. High CR at this interface is attributed to few physical contact points between the carbon fibers in the DM and the carbon particles at the plate surface. In the uncompressed state, the DM is only 20 to 25% by vol. fiber, the remainder air. The surface of a composite plate may contain anywhere from 30 to 90% carbon. Hence, at low compressions, the probability of having few fiber-to-carbon contact points and, in turn, a large CR is high. If the compression pressure is increased, the DM density and the number of contact points increases, thereby reducing the CR. Increasing the compression pressure is, however, a poor solution. It is more advantageous to compress stacks at low pressures to reduce the mass-transport overpotentials and to reduce the mass and size of the bulky end and side plates, which are used to hold the stack under compression. A better alternative is to use a more electrically conducting layer, that is, a conductive-tie layer, at the DM/plate interface that "short-circuits" the flow of current. The use of a conductive-tie layer becomes increasingly more important as we attempt to reduce the filler loadings for improved mechanical properties.

Results and discussion (experimental study)

Bulk Resistance (Flat Design). The materials described above were compression molded using the flat design, cut into 2.5 cm × 2.5 cm × 2 mm coupons, and sanded slightly to remove any polymer skin. The transverse and axial resistivities were measured using the four-point testing procedure mentioned above. Table 6 presents the results. Columns 2 through 4 show that all the materials are electrically anisotropic ($K_a > K_t$), indicating that the flakes/fibers are aligned preferentially in the axial direction. This is a desired characteristic, since the more conductive and longer axial axis of the filler particle will align in the land-to-land direction.

The values in columns 5 and 6 indicate that it is possible to achieve less than 30 mohm·cm^2 resistance at a plate thickness of 2 mm, provided good alignment is achieved with the B4 design and provided the CR is negligible. The values were calculated based on the bulk properties in columns 2 and 3 *and a zero contact resistance*. The values represent the best-case scenario of achieving low plate resistance. If the B4 design is poor and does not promote any significant through-

Table 6. Electrical Properties of Plate Materials

Material	Transverse Resistivity $1/K_t$ (ohm·cm)	Axial Resistivity $1/K_a$ (ohm·cm)	Anisotropy K_a/K_t	Transverse Resistance* 2 mm Plate (mohm·cm^2)	Axial Resistance* 2 mm Plate (mohm·cm^2)	Resistance Ratio Compared to Material C	
						Transverse	Axial
EZ	0.060	0.033	1.8	12.0	6.7	3.6	8.1
PG15	0.163	0.100	1.6	32.5	20.0	9.6	24.4
PAN	0.241	0.047	5.1	48.2	9.5	14.3	11.5
A	0.136	0.032	4.3	27.2	6.4	8.0	7.8
B	0.067	0.009	7.2	13.4	1.9	4.0	2.3
C	0.017	0.004	4.1	3.4	0.8	1.0	1.0

*Bulk only.

plane fiber orientation (similar to the flat design), then high through-plane resistance results, as shown in column 5. This suggests that only materials PG15 and PAN would not meet the resistance target. If, however, the B4 design is good and significant through-plane fiber orientation occurs (column 6), that is, the in-plane orientation of the flat design becomes the land-to-land orientation of the B4 design, then all the materials would meet the resistance target.

Contact Resistance (Flat Design). Unfortunately, the CR between the surfaces of these plate materials and the DM are not negligible, making it more difficult to meet the resistance target. Figure 12 illustrates large CRs associated with the 2 mm thick PAN material in both the axial and transverse directions. The CRs were calculated by subtracting the calculated bulk resistances (columns 5 and 6; Table 6) from the *measured* total resistances. The CRs are large and contribute significantly to the total resistances, particularly at low pressures. Thus, although the axial bulk resistance contribution for the PAN is only 9.5 mohm·cm^2, the high CR contribution does not enable the resistance target of 30 mohm·cm^2 to be achieved, even at 2,068 kPa and with good alignment. For material C, which is the most conductive material used in this study, the CR is significantly smaller, but is still the dominant resistance, as shown in Figure 13. Material C meets the resistance target throughout the pressure range used in both the axial and transverse directions. Alignment is not necessary with this material. Likewise, for materials A and B, the CRs dominate. The resistance target can be met with material A at pressures exceeding 517 kPa (in both the axial and transverse directions), and with material B at pressures exceeding 517 kPa (transverse direction) and 172 kPa (axial direction).

Figure 12 also illustrates the effective use of a silver conductive-tie layer (CTL) to reduce the CR. Silver-filled epoxy adhesive (Epoxy Technology; 60 Ag v/o) was painted onto the surface of the PAN material. The CR was significantly reduced, especially at low pressures. Now PAN can meet the resistance target at pressures greater than 1.03 MPa, assuming good alignment is achieved. A silver CTL was used to demonstrate the CTL effect on CR. In practice, silver would not be used in a fuel cell because it is electrochemically unstable. However, CTL materials such as Au and graphite are stable and can be applied onto composite plate surfaces, and onto organic-coating surfaces that protect metal plates (Blunk et al., 2001b).

Alignment Effect (2 mm Mold Insert). Resistances measured in the second set of experiments are shown in Table 7 for the different plate designs. These are total resistances (contact plus bulk). A silver CTL was used on all samples. Five samples of each material were tested at 1.4 MPa compression pressure. The average resistance (in brackets) and the range of resistances are listed. The % improvement of the B4 design over the other designs is based on the average resistance values. The B0 and B4 samples were molded in the 2 mm insert. The extra land height was removed from the B4 sample using 120-grit silicon carbide paper. The flats samples were molded in the 2 mm flat mold, sanded, and then ma-

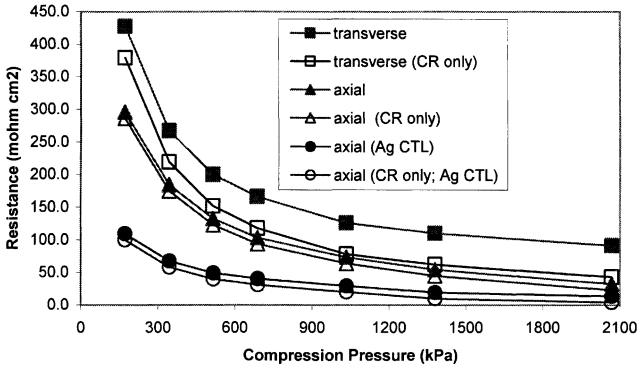

Figure 12. Material PAN- Contact resistance contribution in transverse and axial directions for a 2 mm thick sample.

Effect of a silver conductive-tie layer (Ag CTL) on resistance.

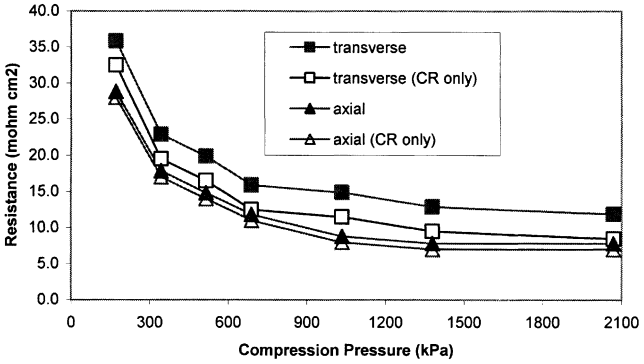

Figure 13. Material C- Contact resistance contribution in transverse and axial directions for a 2 mm thick sample.

Table 7. Resistance for the Flat, B0, and B4 Plate Designs (at 1.38 MPa)

Material	Flat Design (mohm·cm^2)	B0 Design (mohm·cm^2)	B4 Design (mohm·cm^2)	% Improvement B4 vs. Flat	% Improvement B4 vs. B0
EZ	[56] 49–70	[51] 48–61	[45] 39–54	24	13.3
PG15	[160] 145–173	[152] 140–159	[128] 111–152	25	18.8
PAN	[133] 125–146	[91] 82–124	[38] 34–55	250	139.5

chined with grooves at lengths and depths similar to those produced in the B0 and B4 samples. It is imperative to have similar groove lengths and depths in the samples in order to conduct an accurate design comparison of electrical resistances. The groove geometry affects the current distribution at the sample surface and within the sample, which, in turn, affects the plate resistance.

In agreement with the numerical study, the B4 design is better than the B0 design in enhancing plate conductivity. This is especially true for the least-conductive and most anisotropic PAN material, suggesting that the B4 design enhances through-plane orientation/conductivity and the enhancement increase is larger for highly anisotropic materials. The EZ and PAN materials contain the same PAN-based fiber, but the EZ material also contains carbon-black particles that make it more conductive and isotropic (Table 6).

Alignment Effect (1 mm Mold Insert). The resistances of the materials EZ, PG15 and PAN are high and do not meet the resistance target, even after these materials are aligned in the B4 insert and coated with a silver CTL. Consequently, materials with higher loadings of carbon filler were used—A, B and C.

Figure 14 and Table 8 show the effect of alignment on plate resistance using the B4 and flat designs (1 mm thickness) and four plate materials—PAN, A, B, and C. Grooves were machined into the flat samples. Materials molded in the B4 insert, except for material C, were significantly more conductive than those molded in the flat one. Material C is the most conductive material, and although it is anisotropic and probably aligns well in the desired current-flow direction, the resulting resistance is almost completely dominated by the CR, and thus the alignment effect is not observed.

In Figure 14, the resistances obtained from the B4 design (10 cm×10 cm charge pattern) are similar to those obtained earlier (1.3 cm×10 cm charge pattern) for the PAN material, suggesting that either an injection process or extrusion followed by a compression process can be used. Also, a dramatic reduction is shown in resistance when a silver or a graphite CTL is used. The silver layer was applied using a physical vapor deposition process. Gold can also be used and is preferred since it is stable in a PEM fuel cell. The graphite layer was applied using a high pressure (400 to 550 kPa) "blasting" or impingement process in which graphite particles are sprayed at high velocities and embedded into the plate surface.

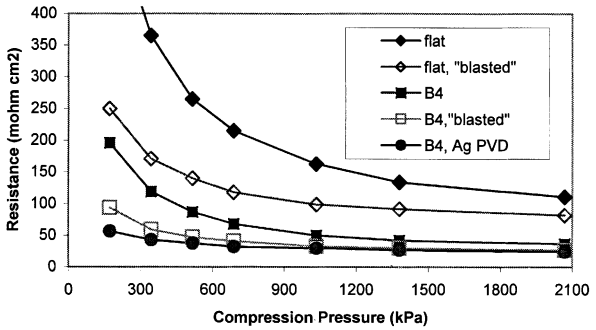

Figure 14. Material PAN- Effect of alignment and the use of a conductive-tie layer on resistance.

1 mm thick sample.

In Table 8, materials A, B and C are assembled into a cooled plate and their resistances presented. Two 1 mm thick plates (anode and cathode) are molded and bonded together using a conductive silver adhesive. The bondline voltage drop is negligible. Materials B and C meet the resistance and thickness targets. Both materials have high loadings of carbon and do not require a CTL. Material B must be aligned to meet the resistance target; material C does not.

Mechanical Properties. A composite plate must meet the resistance (<30 mohm·cm^2) and thickness (<2 mm) targets, and must also possess good mechanical strength. It is difficult to specify the criterion for good mechanical strength. What mechanical property (and magnitude) is needed to reduce the rate of plate breakage to an acceptable level, for example, a 1% scrap rate? Plate breakage depends on many factors, including plate design, handling and packaging methods, molding and demolding operations, stacking pressures, gasketing materials and processes, and so on.

We measured here the flexural properties of three high-graphite-filled composite plates that are currently used in stacks—HG1, HG2 and HG3—and compared these with those exhibited by EZ, PAN, A, B, and C. These HG materials contain between 75 and 90% graphite (by vol.). They are highly conductive (20 to 30 mohm cm^2 at 1.38 MPa) and brittle, require no CTL, and are found to break frequently at a plate thickness of 1.5 to 3.0 mm. The three-point flexural method (ASTM D790) at a cross-head speed of 0.002 cm/s was used to measure flexural properties. Five samples per material were tested. Flexural strength and maximum extension are important attributes when evaluating plate materials. High values for both are desired, and their acceptance magnitudes still need to be determined.

Table 8. Effect of B4 Plate Design on Resistance at Various Compression Pressures (1 mm Insert)

	Resistance (mohm·cm^2)					
Compression (MPa):	0.345		0.69		1.38	
Material	Flat	B4	Flat	B4	Flat	B4
PAN	365	119	215	68	134	42
A (silver CTL)	105	63	77	45	63	35
B	54	40	42	20	34	19
C	40	35	27	27	22	23

Table 9. Flexural Properties of Plate Materials at 21°C

Material	Max. Load at Break (N)	Flexural Strength (MPa)	Flexural Modulus (GPa)	Extension at Max. Load (cm)
HG1	28.9	44.1	12.7	0.28
HG2	28.0	44.1	30.4	0.12
HG3	28.5	40.0	10.2	0.27
EZ	66.3	82.7	16.9	0.57
PAN	18.7	28.9	10.1	0.20
A	38.7	60.7	16.1	0.35
B	17.3	28.9	24.6	0.14
C	21.8	24.1	9.1	0.14

The values in Table 9 (average of five samples) indicate that there is no significant property difference between the HG materials and materials B and C—the ones that meet the thickness and resistance targets. They all contain high filler loadings. Material A (when aligned) almost meets the resistance target and shows higher strength and extension values, which could be attributed to the long carbon fibers used in its formulation. Material EZ exhibits good flexural properties, but is not conductive enough.

Conclusions and Summary

The electrical resistance of composite plates can be reduced significantly using high-aspect-ratio conductive fillers, a fiber/flake alignment process, and a conductive-tie layer (CTL). The alignment process reduces the bulk resistance in the current-flow direction, and the CTL reduces the contact resistance at the plate-to-diffusion medium interface. The bulk resistance reduction is more pronounced with increasing conductive filler anisotropy and decreasing filler loading. The contact resistance reduction is more pronounced at low filler loadings. Unfortunately, however, the amount of reduction is still not enough at the low loadings required for good mechanical plate properties. Loadings of more than approximately 50% (by vol.) are required to meet the resistance and thickness targets.

The B4 geometry does enhance material orientation and conductivity in the current-flow direction, compared with the conventional B0 and flat-plate geometries, but not enough. Electron transport with the B4 geometry is predominantly in the transverse direction of the filler particles. The fibers/flakes align in the primary material-flow (in-plane) direction and, thus, the electrons must conduct in the more resistant transverse direction of the fiber (radial) or flake (thickness), and must "tunnel" through a large number of insulating polymer gaps in order to conduct through the plate thickness.

Ideally, if the B4 design generated a "perfect" land-to-land orientation pattern, the discrete conductive fibers would align in the current-flow direction, and, at relatively low loadings, contact each other to form "continuous" fibers extending through the plate thickness. Good mechanical properties could then be realized since only 1% (by vol.) of a continuous, pitch-based fiber (10^{-4} ohm·cm axial resistivity) is required to achieve the plate resistivity target (10^{-2} ohm·cm). A CTL would then be applied to reduce the contact resistance.

Low concentrations of conductive filler (less than approximately 30% by vol.) are required to obtain significant gains in flexural plate properties. To achieve high conductivities at these concentrations, the "imperfect" B4 design, a CTL, and the following should be used:

(1) Higher concentrations of longer carbon/graphite fibers. Material A contained 10% (by vol.) of 1.2 cm long fibers and exhibited good conductivity and flexural properties. A paper making process or a sheet molding process may work well with these types of materials in order to produce an axial-oriented charge material for the alignment mold.

(2) An extrusion process to obtain unidirectional fiber alignment in the charge material prior to the alignment process. The charge can be positioned in the mold with the fiber directed normal to the long axes of the grooves, and then stamped/molded to generate still higher through-plane orientation.

(3) Continuous fibers that extend through the thickness of the plate (Lisi et al., 2002).

Literature Cited

Advani, S. G., and C. L. Tucker, III, "The Use of Tensors to Describe and Predict Fiber Orientation in Short Fiber Composites," *J. Rheol.*, **31**, 751 (1987).

Balko, E. N., and R. J. Lawrance, "Carbon Fiber Reinforced Fluorocarbon-Graphite Bipolar Current Collector-Separator," U.S. Patent No. 4339322, 13 (July, 1982).

Blunk, R. H. J., C. L. Tucker, III, Y. Yeong-Eun, and D. J. Lisi, "Fuel Cell Separator Plate Having Controlled Fiber Orientation and Method of Manufacture," U.S. Patent Application No. USSN 09/871,189 (filed May 31, 2001a).

Blunk, R. H. J., M. H. Abd Elhamid, Y. M. Mikhail, and D. J. Lisi, "Low Contact Resistance PEM Fuel Cell," U.S. Patent Application No. USSN 09/997,190 (filed Nov. 20, 2001b).

Brooks, A. N., and T. J. R. Hughes, "Streamline Upwind/Petrov-Galerkin Formulations for Convection Dominated Flows with Particular Emphasis on the Incompressible Navier-Stokes Equations," *Comput. Methods in Appl. Mechanics and Eng.*, **32**, 199 (1982).

Busick, D. N., and M. S. Mahlon, "Low-Cost Composite Materials for PEFC Bipolar Plates," *Fuel Cells Bulletin No. 5*, Los Alamos National Laboratory USA (Feb., 1999).

Carmona, F., P. Prudhon, and F. Barreau, "Percolation in Short Fibres Epoxy Resin Composites: Conductivity Behavior and Finite Size Effects Near Threshold," *Solid State Communications*, **51**, 255 (1984).

Cintra, J. S., and C. L. Tucker, III, "Orthotropic Closure Approximations for Flow-Induced Fiber Orientation," *J. Rheology*, **39**, 1095 (1995).

Davies, D. P., P. L. Adcock, M. Turpin, and S. J. Rowen, "Stainless Steel as a Bipolar Plate Material for Solid Polymer Fuel Cells," *J. of Power Sources*, **86**, 237 (2000).

Dresselhaus, M. S., G. Dresselhaus, K. Sugihara, I. L. Spain, and H. A. Goldberg, *Graphite Fibers and Filaments*, Springer Series in Materials Science, New York (1988).

Engelman, M., *Fidap 7.0 Theory Manual*, 1st ed., Fluid Dynamics International, Inc., Rcho STA Marg, CA (1993).

Fronk, M. H., R. L. Borup, B. K. Brady, and S. J. Hulett, "Corrosion Resistant Contact Element for a PEM Fuel Cell," U.S. Patent Application 09/456,478 (filed Dec. 7, 1999).
Grunlan, J. C., W. W. Gerberich, and L. F. Francis, "Lowering the Percolation Threshold of Conductive Composites Using Particulate Polymer Microstructure," *J. of Appl. Polymer Sci.*, **80**, 692 (2001).
Hornung, R., and G. Kappelt, "Bipolar Plate Materials Development Using Fe-based Alloys for Solid Polymer Fuel Cells," *J. of Power Sources*, **72**, 20 (1998).
Larminie, J., and A. Dicks, *Fuel Cell Systems Explained*, Wiley, New York (2000).
Lisi, D. J., R. H. J. Blunk, M. H. Abd Elhamid, and Y. M. Mikhail, "PEM Fuel Cell Separator Plate," U.S. Patent Application USSN 10/074,913 (filed Feb. 11, 2002).
Malliaris, A., and D. T. Turner, "Influence of Particles Size on the Electrical Resistivity of Compacted Mixtures of Polymeric and Metallic Powders," *J. of Applied Physics*, **42** (Feb., 1971).
Patton, T. C., *Paint Flow And Pigment Dispersion*, Wiley, New York (1979).
Sichel, E. K., *Carbon Black-Polymer Composites*, Marcel Dekker, New York (1982).
Tchoudakow, R., O. Breuer, and M. Narkis, "Conductive Polymer Blends With Low Carbon Black Loading: Polypropylene/Polyamide," *Polymer Eng. and Sci.*, **36** (May, 1996).
VerWeyst, B. E., C. L. Tucker, III, P. H. Foss, and J. F. O'Gara, "Fiber Orientation in 3-D Injection Molded Features: Prediction and Experiment," *Int. Polymer Processing*, **14**, 409 (1999).
VerWeyst, B. E., "Numerical Predictions of Flow-Induced Fiber Orientation in 3-D Geometries," PhD Thesis, University of Illinois at Urbana-Champaign, Urbana (1998).
Yi, X. S., G. Wu, and D. J. Ma, "Property Balancing for Polyethylene-based Carbon Black-filled Conductive Composites," *Appl. Poly. Sci.*, **67**, 131 (1998).
Zhang, M., W. Jia, and X. J. Chen, "Influences of Crystallization Histories on PTC/NTC Effects of PVDF/CB Composites," *Appl. Poly. Sci.*, **62**, 743 (1996).

Manuscript received Feb. 25, 2002, and revision received July 31, 2002.